

Core holes, charge disorder, and transition from metallic to plasma properties in ultrashort pulse irradiation of metals

DIMITRI V. FISHER,¹ ZOHAR HENIS,¹ SHALOM ELIEZER,¹ AND JUERGEN MEYER-TER-VEHN²

¹Plasma Physics Department, Soreq NRC, Yavne, Israel

²Max-Planck-Institut für Quantenoptik, Garching, Germany

(RECEIVED 30 March 2005; ACCEPTED 10 August 2005)

Abstract

We study the details of a gradual change in electron properties from those of a nearly-free-electron (NFE) metal to those of a strongly-coupled plasma, in ultrashort pulse energy deposition in solid metal targets. Time scales shorter than those of a target surface layer expansion are considered. Both the case of an optical laser (visible or near infrared wavelengths range) and of a free electron laser (vacuum ultraviolet or X-ray) are treated. The mechanisms responsible for the change in electron behavior are isochoric melting, lattice charge disordering, and electron mean free path reduction. We find that the transition from metal to plasma usually occurs via an intermediate stage of a charge-disordered solid (solid plasma), in which ions are at their lattice sites but the ionization stages of individual ions differ due to ionization from localized bound states. Charge disordered state formation is very rapid (typically, few femtoseconds or few tens of femtoseconds). Pathway to charge-disordered state differs in simple metals and in noble metals. Probabilities are derived for electron impact ionization and 3-body recombination of a bound ionic state in solid-density medium, applicable both in metal and in plasma regime. An evolution of energy coupling between electron and ion subsystems, from metallic electron-phonon (e-ph) to plasma electron-ion (e-i) coupling, is considered. Substantial increase in coupling parameter is expected as a result of charge disorder.

Keywords: femtosecond; metal plasma transition; charge disorder; ionization cross-section

1. INTRODUCTION

Interaction of an ultrashort laser pulse with metal surface leads to a rapid increase in electron temperature, whereas the thermalization between electron and ion subsystems occurs on a substantially longer time-scale (Anisimov *et al.*, 1967, 1974). At laser intensities of 10^{12} to 10^{15} W/cm², for pulse duration of a few tens of femtoseconds, electron temperature T_e typically reaches 1 to 100 eV, while ions remain essentially cold in the duration of the laser pulse. In that situation, a significant redistribution occurs of electrons by their energy states. The ensuing modification of electron charge distribution and lattice potential may facilitate ultrafast melting, or even result in a nonthermal melting of the irradiated material. Ultrafast and/or nonthermal melting facilitated by depopulation of covalent-bonding orbitals was observed in several semiconductors (Shank *et al.*, 1983; Tom *et al.*, 1988; Saeta *et al.*, 1991; Sokolowski-Tinten

et al., 1995, 1998; Siders *et al.*, 1999; Cavalleri *et al.*, 2001; Lindenberg *et al.*, 2005), C (Reitze *et al.*, 1992), and Ga (Uteza *et al.*, 2004), see review by Bennemann (2004). Ultrafast melting phenomenon was extensively studied theoretically (Stampfli & Bennemann, 1992; Rethfeld *et al.*, 2002, 2004), and reproduced in molecular dynamics simulations (Silvestrelli *et al.*, 1996; Gambirasio *et al.*, 2000; Jeschke *et al.*, 2001; Dumitrica & Allen, 2002). Softening of phonon modes was observed in Te (Hunsche *et al.*, 1995) and Bi (DeCamp *et al.*, 2001). Ultrafast thermal melting of Te was observed in (Ashitkov *et al.*, 2002). Significant reflectivity *increase* on a subpicosecond time-scale, incompatible with Drude model and interpreted as melting, was detected in W (Wang & Downer, 1992). For self-absorption measurements or short-delay pump-probe absorption measurements, caution must be exercised to discriminate between suppression of interband absorption in a solid metal and an ultrafast melting of the metal (Fisher *et al.*, 2002).

Transient increase in Al reflectivity at 800 nm pumping/probing wavelength was observed by Guo *et al.* (2000) in pump-probe experiments. Difference in target damage effect

Address correspondence and reprint requests to: Dimitri V. Fisher, Plasma Physics Department, Soreq NRC, Yavne 81800, Israel. E-mail: dimitrifisher@yahoo.com

from 800 nm and 400 nm wavelength pulse was also reported *ibidem*. An increase in Al reflectivity at 800 nm wavelength, and absence of such increase at 400 nm wavelength, were observed by Fisher *et al.* (2002) in self-absorption experiments. Two alternative explanations for the experimental findings were provided in these works. Guo *et al.* (2000) suggested a nonthermal melting of Al, associated with pumping of a bonding-to-antibonding-state interband transition, as an explanation for their experimental results. This hypothesis was further investigated by Youn *et al.* (2004). Fisher *et al.* (2002) have, on the other hand, suggested an electron impact broadening of the interband absorption peak, without a loss of crystalline order, as an explanation for their experimental results. The fact that the increase in Al reflectivity at 800 nm was observed by Fisher *et al.* (2002) to occur on a time-scale of about 50 fs or shorter, at modest laser intensities, agrees with the impact broadening hypothesis, but can hardly be explained by a nonthermal melting. The controversy was eventually laid to rest by the experimental findings of Siwick *et al.* (2003) that rule out the nonthermal melting hypothesis of Guo *et al.* (2000). In Siwick *et al.* (2003) the melting of Al heated by a laser pulse of 800 nm wavelength was found to occur thermally, on a picosecond time-scale.

As the electron temperature increases, the electron-electron (e-e) and electron-ion (e-i) energy and momentum relaxation times characteristic of a periodic-lattice electron behavior must be replaced continuously by the relaxation times characteristic of a nonideal-plasma electron behavior. Although that transition was expected in theory (Lee & More, 1984; Mott, 1990) and observed in experiment (Milchberg *et al.*, 1988; Ng *et al.*, 1994; Price *et al.*, 1995), the details of mechanism, conditions and time-scale of metal-to-plasma electron transition are not known. In the present work we attempt to fill this gap.

It is generally accepted that the exceedingly large probabilities for elastic electron collisions at $T_e \sim T_F$ (where T_F is Fermi temperature), at solid metal densities, result in electron mean free path (MFP) with respect to longitudinal momentum relaxation being of the same order as the typical interionic distance a . The electron longitudinal momentum relaxation rate ν is then approaching u_e/a , where u_e is the characteristic electron velocity. This is the resistivity saturation (also referred to as minimal MFP, minimal conductivity, or Ioffe-Regel) regime (see Chapter 1.6.3 in Mott, 1990). However, very little is known on the details of this transition: how the e-ph interaction is replaced by e-i interaction, how the Umklapp electron-electron scattering dies out, and so on. Also, the details of the transition from (a relatively low) e-ph energy exchange rate to (a relatively high) e-i energy exchange rate, as well as the actual mechanism(s), T_e values, and time-scales on which this transition occurs in various metals remained largely unknown until recently or until now. Attempts to evaluate theoretically the e-i energy exchange rate in a solid target with $T_e \sim 1 - 100$ eV and $T_i < 1$ eV have lead, under different approximations,

to results varying by well over an order of magnitude for the same conditions (Dharma-wardana & Perrot, 1998, 2001; Hazak *et al.*, 2001; Gericke *et al.*, 2002). The key to understanding the e-i energy exchange physics, under the conditions considered is, again, the knowledge of the details of mechanism, conditions, and time-scale of the gradual transition in the conductivity electron properties from nearly-free-electron (NFE)-like to strongly-coupled-plasma-like. As we explain below, this gradual transition involves usually not only the conductivity electrons, but rather the core-state electrons as well.

This work is structured as follows. In Section 2 we consider the mechanisms for lattice periodicity breakdown and for gradual transition from metal-like to plasma-like electron behavior (electron metal-to-plasma transition, eMPT) in metal targets subjected to an ultrashort radiative energy deposition. In Sections 3 to 5, we study in detail the core-state electron impact ionization and three-body (Auger) recombination processes which, as we show, dominate the eMPT in most metals. In Sections 6 to 9, we demonstrate the important differences in eMPT mechanisms between various metallic elements. Three distinct categories of normal metals are found with respect to detailed mechanisms of eMPT under ultrashort laser irradiation. Metals with relatively deep-lying weakest-bound core states (Li, Be, Na, Mg, Al, K, Ca) form the first category. “Relatively” here is defined by comparison with the Fermi energy value in the metal under consideration. Metals with relatively shallow-lying weakest-bound core states (Zn, Cd, Sn, Pb) form the second category. Noble metals Cu, Ag, Au, in which d-band states localize with increasing electron temperature (Fisher *et al.*, 2004, 2005), form the third category. Transitional metals and semimetals are not considered in this work, and will be considered separately. Energy exchange rate between electron and ion subsystems is discussed in Section 7.

We use cgs units in all expressions. In the text, values of particle energies and temperatures are given for convenience in units of electron-volt rather than, respectively, erg or Kelvin.

2. PERIODICITY BREAKDOWN

Fundamental differences exist between electronic properties of a metal and electronic properties of a plasma, at the same ion number density and temperature. Electron transport properties and electron-ion energy exchange rate in metal are governed by lattice periodicity effects on (quasi-) electron states, so that the energy and momentum exchange occurs between collective perturbations of conductivity electron distribution (quasielectrons), and ion distribution (phonons). In plasma, on the other hand, energy and momentum exchange can be described as occurring between individual electrons and ions, in pair collisions, with an environment providing merely a screening background. The key to the transition from quasiparticle to individual-particle picture lies in the relation of the quasiparticle decay rate (in energy

units) to the quasiparticle energy. For the quasiparticle picture to be valid, the former must be much smaller than the latter (Abrikosov, 1972). In other words, periodic-lattice electron behavior breaks down and eMPT occurs when (quasi-)electron total collision frequency, in energy units, is no longer much smaller than the electron Fermi energy.

There are five mechanisms by which the periodic-lattice behavior of conductivity electrons can break down in femto-second laser-matter interaction. The mechanisms are as follows.

(1) Ultrafast isochoric melting. In metals irradiated by an ultrashort laser pulse the melting may occur either with an expansion of the free surface of the target (heterogeneous melting), or, provided the overheating of the solid is substantial, isochorically (homogeneous melting), see (Rethfeld *et al.*, 2004). The mechanism we consider in this paragraph is the isochoric, homogeneous melting; lattice disordering mechanisms involving the free surface are outlined in paragraph (5) below. In NFE metals, homogeneous melting occurs as a result of energy transfer from electrons (they are heated by laser radiation) to lattice ions. As mentioned in the Introduction, in non-NFE metals and in semiconductors the thermal redistribution of electrons over energy levels changes the spatial charge distribution in the lattice and leads to weakening of covalent bonding. The weakened bonding facilitates ultrafast thermal melting. The spatial charge redistribution can induce non-thermal melting in not closely packed lattices. For NFE metals, on the other hand, conductivity electron spatial distribution is much closer to uniform even at low temperatures. Then, a shift of an ion from its equilibrium lattice location occurs on the time scale of one or few phonon periods, 10^2 - 10^3 fs, after isochoric melting ion temperature has been reached. It is important to stress that melting alone does not produce an eMPT. It is well known that a room-pressure isobaric equilibrium melting of a metal does not destroy a short-range lattice order, and thus produces only a modest increase in ν across the melting point. Relation $\nu \ll u_e/a$ certainly remains valid. Laser-induced ultrafast isochoric melting occurs at higher ion temperatures and may have a stronger effect on the short-range order, eliciting stronger increase in ν . Still, an eMPT can not be produced by melting alone; the joint action of some (or all) of the mechanisms listed below is required.

(2) Charge disorder (Fisher *et al.*, 2004, 2005). Ionization of localized core states (in simple metals) or localization of d-band states (in noble metals) with increasing T_e produce ions in a variety of ionization stages occupying individual lattice sites. Ions remain positioned at their lattice sites (at least for some time, estimated to be of the order of 100 fs), but their charge states vary from site to site in a random fashion. Lattice translational symmetry is thus lost even though the geometric ion ordering persists. This is a solid plasma, a charge-disordered solid state. At comparable abundances of two or more different ionization stages, the loss of short-range order is complete. Individual impact ionization events occur on a time-scale of the knocked-out electron

evacuation from its parent ion potential well, that is, $a/u_e \sim 0.1$ fs. However, charge disorder emerges only when the abundance of the next ionization stage becomes significant ($\geq 1\%$). It may take ~ 1 to 100 fs, depending on ionization rate, after T_e reaches sufficiently high values (1 to 20 eV). The details of this mechanism are considered in the Sections 3 to 9.

(3) Reduction in conductivity electron MFP due to the increasing collision rate. A typical linear size L of an electron wave-packet envelope can not significantly exceed the MFP. The MFP, and thus L as well, can become as small as a , thereby destroying Bloch state structure. For ν this phenomenon produces resistivity saturation. The values of ν and L are determined by T_e and, at $T_e \lesssim 1$ eV, also by an ion temperature T_i (Fisher *et al.*, 2002). In absence of charge disorder, resistivity saturation occurs usually as T_e approaches Fermi temperature (Milchberg *et al.*, 1988; Price *et al.*, 1995; Fisher *et al.*, 2002). Time scale for electron MFP reduction is given by the inverse of the electron total collision frequency, which is sub-femtosecond in the vicinity of resistivity saturation regime. Time scale on which T_e changes is significantly longer in most cases, and determines therefore the resistivity saturation onset time.

The three aforementioned mechanisms can operate equally well in the metal bulk and on the metal surface, as they involve neither ion density change nor deviation from a local charge neutrality. There exist another two mechanisms that can affect the metallic electron properties of the target. Those two mechanisms involve explicitly the free target surface.

(4) The local breach of charge neutrality due to the escape of fast electrons from the target surface into the void, and the associated production of strong electric and magnetic fields (Gamaly *et al.*, 2002). The effect of the strong surface fields on the electron states and transport inside the target, in the laser intensities range considered here ($10^{12} - 10^{15}$ W/cm²), remains largely uninvestigated as far as we know.

(5) An anisotropic expansion of the surface target layers normally to the free surface of the target (Eliezer, 2002, 2005; Eidmann *et al.*, 2000). This expansion is driven by the thermal pressure of conductivity electrons heated by the laser radiation absorption to temperatures of a few electron-volts or few tens of electron-volts. Estimates in Fisher *et al.* (2002) show that the typical time-scales for this effect, under our conditions, are in order of $0.1\delta\sqrt{M_i/T_e} \sim 100$ fs, where δ is skin layer thickness, and M_i is ion mass.

In this work we only concentrate on the ‘‘bulk,’’ isochoric mechanisms (1)–(3). As we said in the Introduction, ultrafast melting mechanism (1) is important in semiconductors. Charge disorder mechanism (2) and electron MFP reduction mechanism (3) are dominant in simple metals. Furthermore, we show that there are two alternative pathways to charge disorder, one realized by ionization of the core states and the other realized by localization of the d-band states of noble metals. After the initial isochoric stage, which lasts several tens or hundreds of femtoseconds, expansion of the heated

layers into the void can no longer be neglected, and mechanism (5) becomes important in most systems.

3. IONIZATION OF CORE STATES AND CHARGE DISORDER

Charge disorder in normal metals is produced by ionization of localized core electron states. First we consider metals with core states lying at least several eV below the bottom of the conductivity band. Noble metals (Cu, Ag, Au), in which the d-band energy lies above the bottom of the conductivity band but below the Fermi level, or metals with core states or d-band located close to the bottom of the conductivity band (Zn, Cd, Sn, Pb), are considered in Sections 8 and 9. The charge disordering mechanism is more complicated in those metals.

Both in metals and in plasma the ionization of a bound electron state can occur either by a free electron impact or by photon absorption. At the laser intensities relevant to this work (below 10^{15} W/cm²) multiphoton ionization of core states can be neglected; therefore, for photon energies below the photoionization threshold (optical laser), the only ionization channel is the electron impact ionization (EII) of core states by sufficiently energetic conductivity electrons. For a vacuum-ultraviolet free electron laser (see, e.g., Lee *et al.*, 2002; Ke Lan *et al.*, 2004; Alesini *et al.*, 2004), or any other source of high-intensity femtosecond/attosecond radiation pulses with photon energies above the core state photoionization threshold in the irradiated sample, both EII and photoionization channels must be accounted for.

Finally, in a solid matter bombarded by an intense energetic ion beam (either laser or accelerator produced, see e.g. Malka & Fritzler, 2004; Hoffmann *et al.*, 2005), dynamics of isochoric transition from an ordered solid to a high-energy-density matter is of significant interest. There, on sufficiently short time scales, both charge disordering due to interaction with projectile ions and charge disordering due to EII by hot electrons are expected.

4. IONIZATION OF CORE STATES BY CONDUCTIVITY ELECTRON IMPACT

Here we restrict ourselves to consideration of only the shallowest-lying (weakest-bound) core states of any ion, as core hole abundances even lower than one per ion are already sufficient for the eMPT. Core states considered have binding energies in the range of 15 to 100 eV, depending on the chemical element. Deeper-lying core states are not affected under present conditions. Zero of energy is chosen at the bottom of conductivity band, so that the core states have negative energy (i.e., positive binding energy E_b), and conductivity electron states have positive energy. An EII event occurs when a sufficiently energetic conductivity electron collides with a core-state electron, with energy transfer in the collision exceeding the core state binding energy. Final

states of both electrons belong then in conductivity band, and an ionization degree of the parent ion increases by unity.

As the gradual eMPT is what we are ultimately interested in, we must develop a **unified** description for EII events (their cross-section, probability, and rate) in metal and in plasma. To the best of our knowledge, this was never carried out. The weakest-bound core state in metal is equivalent to an optical electron state of a plasma ion, and the NFE conductivity-band states in metal are equivalent to free electron states in plasma. The core state binding energy in metal is therefore measured relative to the bottom of the conductivity band. Due to density-dependent screening effects, the binding energy for the same ionic state in metal and in dilute plasma differ (see, for example, Johansson & Martenssen, 1980). The EII cross section must be scaled to the correct binding energy (Salzmann, 1998). The appropriate expression for the EII cross-section $\sigma_{EII}(E)$, where E is the incident electron energy, is presented at the end of this Section. For now, it is sufficient to state that $\sigma_{EII}(E)$ is a smooth finite non-negative function of E , and

$$\begin{aligned} \sigma_{EII} &= 0 & \text{for } E \leq E_b, \\ \sigma_{EII} &\geq 0 & \text{for } E > E_b. \end{aligned} \quad (1)$$

This presumes the absence of excitons in metal under conditions considered here.

To evaluate the probability (per second) P of ionization of a core state in a single ion, we use

$$P \equiv N_e \langle \sigma_{EII}(E) u(E) \Pi(E - E_b) \rangle, \quad (2)$$

where N_e is the number density of conductivity electrons, $u(E)$ is the incident electron velocity, and the average $\langle \rangle$ is over the conductivity electron energy distribution. Π is a Pauli blocking factor accounting for reduction in P due to the significant probability of the electron final state(s) being occupied. The conductivity band is assumed parabolic in the extended zone scheme,

$$E = \frac{\hbar^2 k^2}{2m_e}, \quad (3)$$

with k denoting the (quasi)electron momentum, and with the (quasi)electron mass equal to a free electron mass. Then,

$$u(E) = \left(\frac{2E}{m_e} \right)^{1/2}. \quad (4)$$

The averaging in Eq. (2) is over the energy distribution $g(E)f(E)$ of the incident electron,

$$\langle x \rangle = \frac{\int_0^\infty x(E)g(E)f(E) dE}{\int_0^\infty g(E)f(E) dE} \equiv \frac{\int_0^\infty x(E)g(E)f(E) dE}{N_e}. \quad (5)$$

Here

$$g(E) = \begin{cases} 0 & \text{for } E \leq 0 \\ \left(\frac{m_e}{\hbar^2}\right)^{3/2} \frac{1}{\pi^2} (2E)^{1/2} & \text{for } E \geq 0 \end{cases} \quad (6)$$

is the conductivity electron density of states (in units of $[1 / \text{erg cm}^3]$) in a NFE band with dispersion relation (3), and

$$f(E) = \left[1 + \exp\left(\frac{E - \mu(T_e)}{k_B T_e}\right) \right]^{-1} \quad (7)$$

is the Fermi-Dirac distribution function, where k_B is Boltzmann constant, and μ is electron chemical potential. The values of $\mu(T_e)$ are determined implicitly by the identity

$$N_e \equiv \int_0^\infty g(E)f(E) dE. \quad (8)$$

The EII event is only possible when the final states are vacant for both electrons involved. In contrast to a classical plasma, in nonclassical plasma or in metal the probability for the final states to be vacant may be low. Therefore, in the average (in right-hand side of Eq. (2)) a Pauli blocking factor $0 < \Pi(E - E_b) < 1$ is included, and the expression for EII rate becomes

$$W = N_i P = N_i \int_{E_b}^\infty \sigma_{\text{EII}}(E) u(E) g(E) f(E) \Pi(E - E_b) dE. \quad (9)$$

We estimate the blocking factor $\Pi(E - E_b)$ in the following way. The total energy of the two electrons in the final state is $E - E_b > 0$. The probability to find the final state vacant decreases nearly exponentially as the energy of one of the final states decreases. Thus, the most favorable scattering event with respect to both final states being vacant is the scattering in which final energy of both electrons is approximately equal, each one being given then by $(E - E_b)/2$. Hence, the factor $\Pi(E - E_b)$ may be approximated by

$$\begin{aligned} \Pi(E - E_b) &\approx \left\{ 1 - f\left(\frac{E - E_b}{2}\right) \right\}^2 \\ &= \left\{ 1 + \exp\left[-\frac{\left(\frac{E - E_b}{2} - \mu\right)}{k_B T_e}\right] \right\}^{-2}. \end{aligned} \quad (10)$$

It approaches unity, of course, as E increases. It also approaches unity for any E at large T_e due to a drop in $\mu(T_e)$. In a low- T_e limit, $k_B T_e \ll \mu$, Eq. (10) is straightforward to derive; this is done by assuming any realistic form of differential EII cross-section $d\sigma/d\epsilon$ (where $0 \leq \epsilon \leq E - E_b$ is the energy of ejected electron) and integrating over ϵ . A prefactor close to unity appears then in the low- T_e limit of the right-hand side

of (10). The prefactor depends on E, E_b, μ , as well as on the details of the functional form of $d\sigma/d\epsilon$. Most important, however, it does *not* depend on T_e . We neglect the said prefactor altogether.

We note that N_e does not appear explicitly in Eq. (9). Instead, it enters implicitly through the value of $\mu(T_e)$, which appears in Eq. (7) for $f(E)$. In classical plasmas $f(E) \ll 1$ for all $E \geq 0$. In that limit we find $\Pi(E - E_b) \approx 1$ for all $E \geq E_b$, and $f(E) \approx \exp[(\mu - E)/k_B T_e]$. Using the nondegenerate free-electron asymptote $\mu(T_e) \approx 1.5 k_B T_e \ln[4/3\sqrt{\pi}(\hbar^2/2m_e)(3\pi^2 N_e)^{2/3}(k_B T_e)^{-1}] < 0$ one finds $f(E) \sim N_e T_e^{-3/2} \exp(-E/k_B T_e)$, hence the familiar explicit factor N_e in EII probability in classical plasma.

In the above model for P , the use of a constant value for E_b is only justified as long as the depletion of the core state is not too large (say, no more than 10% vacancies abundance in the core state; for example, no less than 5.4 electrons on average per ion in the 2p state of Al). The abundance of holes (vacancies) in a core state is defined here as a ratio of the number of vacant electron states to the total number of electron states. At larger vacancy abundances, the reduction in nucleus screening for the remaining core electrons becomes important and E_b increases. This effect can be accounted for in equilibrium, by the following extension of the model. The equilibrium core hole abundance $h(T_e)$ is evaluated by including a narrow core state in the density of states, Eq. (6), and recalculating the chemical potential from Eq. (8) with N_e now including the core electrons as well; then $h = 1 - f(-E_b)$. Values of $E_b(T_e)$ may be found using INFERNO model (Lieberman, 1979, 1982).

For a laser pulse not much longer than the typical equilibration times, on the other hand, the equilibrium number of vacancies in the core state is not reached, and the core states are thus overpopulated for the given T_e (i.e., actual vacancy abundance is lower than h). In the nonequilibrium case it is possible to solve rate equations for h , and to use $E_b(h)$ as above; such a procedure, however, is beyond the scope of the present work. The hole population equilibration time is estimated in Section 6.

The following point must be clarified. Since the core state is localized, not all ions have the same number of core electrons. Consequently, the notion of $E_b(T_e)$ is meaningful only in the average sense, as explained in the Appendix of Lieberman (1979). Simply put, ions with $K = 1, \dots, q$ electrons in the core state have different binding energies E_{bK} of the core state. The smaller is K , the larger is E_{bK} . The average $E_b(T_e)$ increases with T_e following the shift in the ionization composition of the matter, so that $E_b(T_e)$ is not far from E_{bK} for the dominant K value at any given T_e . Due to the dependence of free-electron screening on free electron density and temperature, all E_{bK} are also functions of T_e . However, the T_e dependence of E_{bK} is significantly weaker than the T_e dependence of the average $E_b(T_e)$. As we already said, core-hole ion ($K = q - 1$) abundance $\sim 1\%$ in metal is sufficient to produce the charge disorder and the ensuing eMPT. Thus, for normal metals below we assume $E_b = E_{bq}$,

that is, binding energy is that of an electron in a fully occupied core state, unless explicitly stated otherwise. For noble metals the situation with the d-band energy is different, see Section 8.

Let us now turn to the determination of an appropriate expression for $\sigma_{EII}(E)$. In a single ion, the cross-section for a direct EII event may be approximated by Lotz formula,

$$\sigma_{Lotz} = \begin{cases} 0 & E \leq E_b \\ 2.76\pi a_0^2 q \left(\frac{Ry}{E_b}\right)^2 \frac{\ln(E/E_b)}{(E/E_b)} & E \geq E_b \end{cases} \quad (11)$$

see e.g., Pal'chikov and Shevelko (1995). Here a_0 is Bohr radius, q is the degeneracy of the core state, and $Ry = 13.6$ eV is the binding energy of a ground state of an isolated hydrogen atom. Lotz formula was obtained semi-empirically to fit the EII cross-sections measured for multiply charged ions. It was later found to be applicable to majority of direct EII cross sections in dilute ideal plasmas (including EII of weakly charged ions and EII from inner shells) (Griem, 1997). However, Lotz formula in its original form is inapplicable to either metals or dense plasmas. It does not account for the screening of a momentum transfer between electrons in a dense conducting medium. It also does not account for the difference in low-energy conductivity electron wave functions between a condensed matter and a dilute plasma. The latter problem is especially acute for low projectile energy values, $E \approx E_b$. The $E/E_b \gg 1$ nonrelativistic asymptotic (Bethe) form of Eq. (11) is applicable to an atom in dense medium as well as to an atom in dilute plasma. The screening effect of the medium becomes important either in relativistic limit (Fermi, 1940; Sternheimer & Peierls, 1971; Inokuti & Smith, 1982) which is not considered here, or for $E \lesssim \hbar\omega_{pe} = \hbar\sqrt{4\pi N_e e^2 m_e^{-1}}$ (see, for example, Nozieres & Pines (1995) and Murillo & Weisheit (1998)). In most metals, the plasma frequency ω_{pe} obeys $\hbar\omega_{pe} \lesssim E_b$. Thus, both the screening and the continuum wavefunction modification by the dense medium necessitate the amendment of Eq. (11) at the low (near-threshold) projectile energies, $E \sim E_b$. Under present conditions, the σ_{EII} values in medium tend to be lower than for an individual ion. We introduce, therefore, an empirical correction factor $(1 - E_b/E)^Y$ into the EII cross-section,

$$\sigma_{EII} = \begin{cases} 0 & \text{for } E \leq E_b \\ 2.76\pi a_0^2 q \left(\frac{Ry}{E_b}\right)^2 \frac{\ln(E/E_b)}{(E/E_b)} \left(1 - \frac{E_b}{E}\right)^Y & \text{for } E \geq E_b \end{cases} \quad (12)$$

Here $Y > 0$ is a fitting constant depending on the chemical element (and possibly on a lattice structure of metal, for elements in which a number of metallic phases exist). The value of Y can be found from the room-temperature experimental values of the core hole lifetimes, as explained in the

next Section. Note that in the present model Y is independent of T_e . By adopting Eq. (12) we therefore neglect the effect on EII cross-section stemming from changes in electron eigenstates and electron screening with an increasing electron temperature at a given ion density. This is, of course, an oversimplification; however, as T_e increases, the dominant contribution to EII comes from larger E values, and the factor $(1 - E_b/E)^Y$ becomes less important. We stress that Y is a function of ion density, and may be assumed constant only as long as ions remain motionless (as in the present case). In expanding plasmas Y is expected to decrease as N_i decreases, and to approach zero eventually when N_i is low enough for the density effects on EII cross-section to be negligible.

In this work we concentrate on the ionization in metal targets with T_e no larger than, say, 100 eV. This roughly corresponds to laser intensities below 10^{15} W/cm², for a pulse duration of a few tens of femtoseconds. Rapid ionization of target material at higher laser intensities is considered, for example, by Kemp *et al.*, (2004).

For completeness, we note that the EII contribution to stopping of a hot electron in a **cold** metal, and a related problem of an Auger lifetime of a core vacancy in metal at room conditions, have been studied (Almbladh *et al.*, 1989; Schoene *et al.*, 1999; Campillo *et al.*, 2000; Knorren *et al.*, 2001). The results in these publications are obtained by means of detailed band structure calculations, and are inapplicable to the systems with T_e comparable with Fermi temperature or higher.

5. IONIZATION AND RECOMBINATION RATES

The process inverse to EII is the three-body recombination or, synonymously, an Auger process involving two electrons in a conductivity band and a core state hole. The three-body recombination probability and rate are found from the detailed balance requirements for the equilibrium conditions. We consider the simple case of relatively low abundance of holes, such that only $K = q$ and $K = q - 1$ species are present in the system. That is, abundances of species with $K < q - 1$ are negligible. This is the case relevant to eMPT. The equilibrium core hole abundance $h = 1 - f(-E_b)$. There are q core states per ion, and each of those states can be occupied or vacant. Thus, the probability to have a hole in the core state of a given ion equals qh , provided the probability to have more than one core-state hole per ion is negligible. Of course, this approximation is only accurate for $qh \ll 1$. The probability to have no holes in the core state is then $1 - qh$. Rate of EII (in units of events per second per cm³) is given by

$$W = N_q P, \quad (13)$$

where N_q is the number density of ions with no core-state holes (i.e., with q electrons in the core state per ion). In equilibrium,

$$N_q = N_i(1 - qh), \quad (14)$$

where N_i is the total number density of lattice ions. Likewise, three-body recombination rate W_3 is expressed via the three-body recombination probability P_3 by

$$W_3 = N_{q-1} P_3, \quad (15)$$

where N_{q-1} is the number density of ions with one core hole per ion. The physical meaning of P_3 is the inverse mean lifetime, $\langle \tau_h \rangle^{-1} \equiv P_3$, of a hole in a core state of a lattice ion. For equilibrium conditions, N_{q-1} is given by

$$N_{q-1} = N_i qh. \quad (16)$$

In equilibrium between the core state population and the next ionization stage ground state population, $W_3 = W$. Thus, for $qh \ll 1$,

$$P_3 = \frac{1 - qh}{qh} P = \frac{\frac{1}{q} - [1 - f(-E_b)]}{1 - f(-E_b)} P. \quad (17)$$

The three-body recombination occurs in an interaction of two conductivity electrons in presence of an ion with a core-state vacancy. One of the conductivity electrons makes a transition into the vacant core state and the other one takes the excess energy. In the limit $k_B T_e \ll \min(E_b, E_F)$, where $E_F \equiv k_B T_F \equiv \mu(T_e = 0)$, one should expect P_3 to become independent of T_e , since the energy distribution of conductivity electrons becomes nearly independent of T_e at $k_B T_e \ll E_F$. It is easy to show that Eq. (17) yields indeed the correct limiting behavior: $\lim_{T_e \rightarrow 0} P_3 = \text{const}$. The prefactor in Eq. (17) becomes

$$\lim_{T_e \rightarrow 0} \frac{\frac{1}{q} - [1 - f(-E_b)]}{1 - f(-E_b)} = \frac{1}{q} \exp\left(\frac{E_F + E_b}{k_B T_e}\right).$$

To find the limit $\lim_{T_e \rightarrow 0} P$, we must consider two distinct cases: $E_F < E_b$ and $E_F \geq E_b$. Let us first consider the case $E_F < E_b$. Using Eq. (9) for P and Eq. (7) for f , we find

$$\lim_{T_e \rightarrow 0} P_3 = \frac{1}{q} \exp\left(\frac{E_F + E_b}{k_B T_e}\right) \lim_{T_e \rightarrow 0} P = \frac{1}{q} \exp\left(\frac{E_F + E_b}{k_B T_e}\right) \lim_{T_e \rightarrow 0} \int_{E_b}^{\infty} \frac{\left(\frac{2E}{m_e}\right)^{1/2} \left(\frac{m_e}{\hbar^2}\right)^{3/2} \frac{(2E)^{1/2}}{\pi^2} \sigma_{EII}(E) dE}{\left[1 + \exp\left(\frac{E - \mu}{k_B T_e}\right)\right] \left\{1 + \exp\left[-\frac{\left(\frac{E - E_b}{2} - \mu\right)}{k_B T_e}\right]\right\}^2}. \quad (18)$$

In the case under consideration, unity next to $\exp((E - \mu)/k_B T_e)$ is negligible since $k_B T_e \ll E_F < E_b$, $E \geq E_b$, and $\lim_{T_e \rightarrow 0} \mu(T_e) = E_F$. Thus,

$$\begin{aligned} \lim_{T_e \rightarrow 0} P_3 &= \frac{1}{q} \exp\left(\frac{E_F + E_b}{k_B T_e}\right) \frac{2m_e}{\pi^2 \hbar^3} \lim_{T_e \rightarrow 0} \int_{E_b}^{\infty} \frac{\sigma_{EII}(E) E dE}{\exp\left(\frac{E - \mu}{k_B T_e}\right) \left\{1 + \exp\left[-\frac{\left(\frac{E - E_b}{2} - \mu\right)}{k_B T_e}\right]\right\}^2} \\ &= \frac{2m_e}{\pi^2 \hbar^3 q} \lim_{T_e \rightarrow 0} \int_{E_b}^{\infty} \frac{\sigma_{EII}(E) E dE}{\left\{\exp\left[\frac{\left(\frac{E - E_b}{2} - \mu\right)}{k_B T_e}\right] + 1\right\}^2} \\ &= \frac{2m_e}{\pi^2 \hbar^3 q} \int_{E_b}^{E_b + 2E_F} \sigma_{EII}(E) E dE, \end{aligned} \quad (19)$$

independent of T_e . For the case $E_F \geq E_b$, which corresponds to a relatively weakly bound (shallow-lying) core state, one finds in a similar way

$$\begin{aligned} \lim_{T_e \rightarrow 0} P_3 &= \frac{2m_e}{\pi^2 \hbar^3 q} \lim_{T_e \rightarrow 0} \left[\int_{E_b}^{E_F} \exp\left(\frac{E - E_F}{k_B T_e}\right) \sigma_{EII}(E) E dE + \int_{E_F}^{E_b + 2E_F} \sigma_{EII}(E) E dE \right] \\ &= \frac{2m_e}{\pi^2 \hbar^3 q} \int_{E_F}^{E_b + 2E_F} \sigma_{EII}(E) E dE, \end{aligned} \quad (20)$$

independent of T_e , too. Thus, for both cases $\lim_{T_e \rightarrow 0} P_3$ can be described by a single expression

$$\begin{aligned} \lim_{T_e \rightarrow 0} P_3 &= \frac{2m_e}{\pi^2 \hbar^3 q} \int_{\max(E_b, E_F)}^{E_b + 2E_F} \sigma_{\text{EII}}(E) E dE \\ &= 2.76 \pi a_0^2 \left(\frac{Ry}{E_b} \right)^2 \frac{2E_b m_e}{\pi^2 \hbar^3} \\ &\quad \times \int_{\max(E_b, E_F)}^{E_b + 2E_F} \left(1 - \frac{E_b}{E} \right)^Y \ln(E/E_b) dE. \end{aligned} \quad (21)$$

The value of $\lim_{T_e \rightarrow 0} P_3$ depends on N_e both via $E_F \sim N_e^{2/3}$ and via Y . The dependence of P_3 on N_e in this degenerate-conductivity-electrons limit is therefore far more complicated than the trivial $P_3 \sim N_e^2$ dependence encountered in an ideal classical plasma limit.

Eqs. (18) and (21) show that, despite the Pauli blocking, for $k_B T_e \ll E_F$ the dominant contribution to EII probability P comes from slow projectile electrons, $E_b < E \leq E_b + 2E_F$. This underlines the importance of the empirical correction factor $(1 - E_b/E)^Y$ introduced in the previous Section.

6. RESULTS FOR SIMPLE METALS WITH LARGE E_b/E_F

We have calculated $P(T_e)$ and $P_3(T_e)$ for solid-density Li, Be, Na, Mg, Al, K, and Ca. For these metals the ratio $E_b/E_F > 4$. Parameters used in the calculations are presented in Table 1. Elements are listed in the order of increasing atomic number. Values of N_e include conductivity electrons only. Values of the binding energy with respect to Fermi level, $E_b + E_F$, are taken from NIST data tables <http://physics.nist.gov/PhysRefData/FFast/Text/Cover.html>. Values of E_F are obtained from table values for N_e using Eq. (8) at $T_e = 0$. Values of room-temperature hole lifetimes $\langle \tau_h \rangle$ were found in literature, as follows. For Li, we adopted the experimental value of $\langle \tau_h \rangle = \hbar/\Gamma \approx 20$ fs as reported by Citrin *et al.* (1979), where Γ is the lifetime broadening of the core hole state. For Be, no experimental data were found, so we used the value of $\langle \tau_h \rangle \approx 16$ fs obtained by band structure calculations (Almbladh *et al.*, 1989). For Na and Mg we adopted the $\langle \tau_h \rangle$ experimental values of ≈ 70 fs and ≈ 30 fs,

respectively (Citrin *et al.*, 1979; Neddermeyer, 1976). For Al, we adopted the experimental value of $\langle \tau_h \rangle \approx 20$ fs reported by Theis and Horn (1993), see also, Almbladh *et al.* (1989) and Citrin *et al.* (1979). For K, experimental $\langle \tau_h \rangle \approx 44$ fs (First *et al.*, 1988). All the above $\langle \tau_h \rangle$ data are typically accurate to within a factor of 2. Datum for K is accurate to within 15%. For Ca no data were found either experimental or theoretical, so we used a typical value $\langle \tau_h \rangle \approx 20$ fs; this is merely an order-of-magnitude ‘‘guesstimate.’’ Table 1 lists also the fitted Y values for room-density metallic state of Li, Be, Na, Mg, Al, K, and Ca. The Y values were determined by equating the $\lim_{T_e \rightarrow 0} P_3$ value, Eq. (21), to $\langle \tau_h \rangle^{-1}$ for each of the elements. We note the ostensible regularity in Y : the latter seems to grow nearly monotonously with the increasing atomic number.

Calculation results for EII probability P in the aforementioned metals are presented in Table 2. Data are only given for $P > 10^6 \text{ s}^{-1}$. Figure 1 shows $P(T_e)$ for the same metals. Figure 2 shows calculation results for $P_3(T_e)$ in the same metals, up to $qh = 0.1$. One can see that P_3 decreases with increasing temperature. It is important to note that constant E_b and N_e were assumed in the above calculations, which corresponds to core-ionized ion abundance much smaller than unity. As we said, under equilibrium conditions the present values of $P(T_e)$ and $P_3(T_e)$ are only valid for T_e such that the equilibrium core-ionized ion abundance $qh(T_e) \ll 1$. For very short pulses, as long as the hole abundance is substantially lower than in equilibrium, present values of $P(T_e)$ can be used at higher T_e as well (provided the conductivity electrons are thermalized between themselves, i.e., the conductivity electron distribution function can be approximated by Eq. (7)).

Rate with which an equilibrium value h of the core hole abundance is approached, for a given electron temperature T_e , is easy to evaluate. Assuming, as above, that only $K = q$ and $K = q - 1$ species are present in the system, for N_q and N_{q-1} the following rate equations are readily written down:

$$\dot{N}_q = -PN_q + P_3 N_{q-1}, \quad (22)$$

$$\dot{N}_{q-1} = -\dot{N}_q, \quad (23)$$

Table 1. Parameters of weakest-bound core states for several metals

Element	Core State	E_b [eV]	N_e/N_i [-]	N_e [cm ⁻³]	E_F [eV]	q [-]	$\langle \tau_h \rangle$ [fs]	Y [-]
Li	1s (K)	50.0	1	4.63×10^{22}	4.71	2	20	0.8
Be	1s (K)	96.6	2	2.47×10^{23}	14.4	2	16	1.4
Na	2p (L II, III)	28.0	1	2.54×10^{22}	3.15	6	70	1.7
Mg	2p (L II, III)	44.3	2	8.62×10^{22}	7.12	6	30	1.9
Al	2p (L II, III)	61.4	3	1.81×10^{23}	11.7	6	20	2.0
K	3p (M II, III)	15.8	1	1.32×10^{22}	2.04	6	40	1.6
Ca	3p (M II, III)	20.7	2	4.62×10^{22}	4.70	6	?	2.5

Table 2. Calculated probabilities of core state electron impact ionization for several metals

Element	Core State Electron Impact Ionization Probability P [s^{-1}] at Solid Density					
	$T_e = 3$ eV	$T_e = 5$ eV	$T_e = 7$ eV	$T_e = 10$ eV	$T_e = 15$ eV	$T_e = 20$ eV
Li	$<10^6$	1.7×10^9	4.7×10^{10}	5.9×10^{11}	4.6×10^{12}	1.3×10^{13}
Be	$<10^6$	$<10^6$	1.3×10^7	1.7×10^9	8.6×10^{10}	6.6×10^{11}
Na	3.6×10^9	3.7×10^{11}	3.0×10^{12}	1.6×10^{13}	6.3×10^{13}	1.3×10^{14}
Mg	5.9×10^6	7.4×10^9	1.8×10^{11}	2.2×10^{12}	1.8×10^{13}	5.4×10^{13}
Al	$<10^6$	1.1×10^8	8.7×10^9	2.5×10^{11}	4.0×10^{12}	1.7×10^{13}
K	7.5×10^{11}	1.3×10^{13}	4.6×10^{13}	1.3×10^{14}	3.1×10^{14}	4.8×10^{14}
Ca	6.6×10^{10}	3.0×10^{12}	1.8×10^{13}	7.4×10^{13}	2.5×10^{14}	4.8×10^{14}

with the initial condition $N_q(t=0) = N_q^0$, $N_{q-1}(t=0) = N_{q-1}^0 = N_i - N_q^0$. The solution is

$$N_q(t) = N_q^{LTE} + (N_q^0 - N_q^{LTE})\exp(-\Omega t), \quad (24)$$

$$N_{q-1}(t) = N_{q-1}^{LTE} + (N_{q-1}^0 - N_{q-1}^{LTE})\exp(-\Omega t), \quad (25)$$

where

$$N_q^{LTE} = N_i \frac{P_3}{P + P_3} = N_i(1 - qh) \quad (26)$$

and

$$N_{q-1}^{LTE} = N_i \frac{P}{P + P_3} = N_i qh. \quad (27)$$

The hole abundance relaxes to its equilibrium value h at the rate Ω which is given by

$$\Omega = P + P_3. \quad (28)$$

Ω values vary between 10^{13} and $10^{15} s^{-1}$ for the metals considered in this Section.

For a short-range lattice order to be destroyed by charge disordering, the fraction N_{q-1}/N_i of core-ionized ions in the medium must be in excess of, say, $0.1/n \sim 0.01$. Here n is the number of near neighbors of a given ion in the lattice, typically between 4 and 12. To attain these values of N_{q-1}/N_i by means of ultrashort optical laser energy deposition one needs, first of all, to reach T_e such that $qh(T_e) \geq 0.01$. Furthermore, to attain these values of N_{q-1}/N_i on a 100-fs scale or faster, one needs the EII rate $P > 10^{11} s^{-1}$, see Eq. (22). Temperatures at which qh equals 0.001, 0.01, and 0.1 are listed in Table 3. For readers' convenience, Fermi energies of the elements are listed again in Table 3. By looking at Tables 2 and 3, one can immediately see that the charge disorder emerges at $T_e \approx (0.5 - 2)T_F$. That is, the same temperature range as for the minimal conductivity regime. For that reason, it is hard (if at all possible) to detect charge disorder by self-absorption or pump-probe measurements of optical properties of the metals considered in this section. This confirms the conclusion drawn by Fisher *et al.* (2002) that for 50-fs laser pulse irradiation of Al targets at

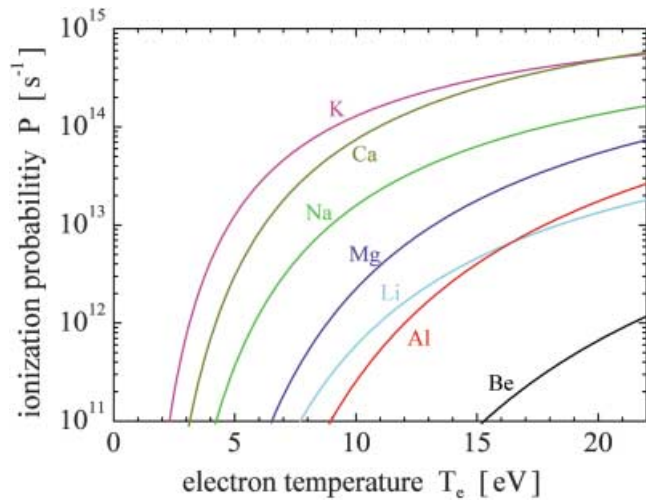


Fig. 1. Calculated probabilities of core state electron impact ionization for several metals.

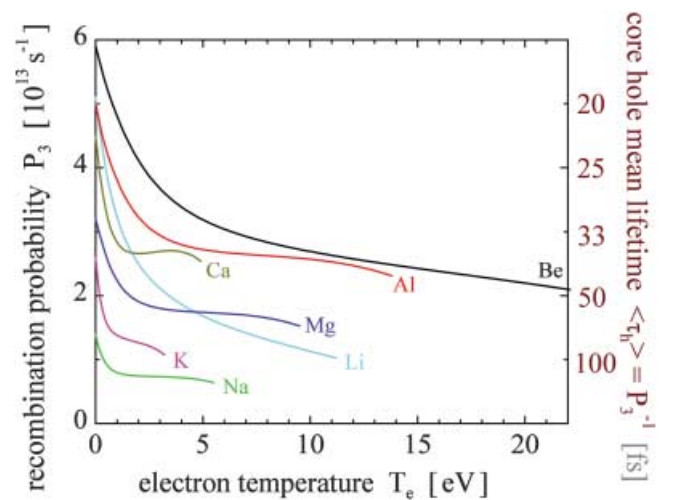


Fig. 2. Calculated probabilities of core vacancy 3-body recombination for several metals.

Table 3. Temperature values corresponding to specified equilibrium core-ionized ion abundances qh

Element	E_F [eV]	$T_e (qh = 10^{-3})$ [eV]	$T_e (qh = 10^{-2})$ [eV]	$T_e (qh = 0.1)$ [eV]
Li	4.71	6.2	8.0	11.2
Be	14.4	13.0	17.1	24.6
Na	3.15	3.2	4.1	5.5
Mg	7.12	5.4	7.0	9.6
Al	11.7	7.8	10.0	13.9
K	2.04	1.9	2.4	3.2
Ca	4.70	2.7	3.5	4.9

intensities below 10^{15} W/cm², at 1.5 eV and 3 eV photon energies, the core state ionization does not affect appreciably the laser pulse absorption coefficient.

Charge disorder can also be produced, temporarily, by a hard ultraviolet or X-ray laser irradiation of a metal sample. To produce an observable charge disorder effect in a relatively cool metal, photons with energy close to the photoionization threshold $E_b + E_F$ are required. Tunability of a free electron laser presents a great advantage in this case. The optimal laser energy deposition should be such that the N_{q-1}/N_i value produced is in the range 0.01 – 0.1. Lower core hole populations are harder to observe, while higher core hole populations yield, upon recombination to equilibrium hole abundances, T_e values that are too high (close to Fermi temperature). At $T_e \approx T_F$ or higher, the ν values, as we said, are close to minimal conductivity value anyway, and the charge disorder effect is not manifested in optical properties. Core hole population thermalization is expected to occur, under the conditions relevant to X-ray induced charge disorder, at a rate of $(1 - 5) \times 10^{13}$ s⁻¹, that is, on a time scale of tens of femtoseconds, see Figure 2.

7. ENERGY COUPLING BETWEEN ELECTRON AND ION SUBSYSTEMS

It is important to stress that the charge disorder being hard to detect *optically* in metals listed in Tables 1–3 does not imply that charge disorder is hard to detect *at all* in these metals. Charge disorder produces a significant increase in electron-ion energy coupling (Fisher, 2005b). Indeed, a solid-density medium with partially degenerate conductivity electrons and *identical* ions in a short-range order may have an e-i energy coupling coefficient significantly lower than a strongly-coupled plasma under the same conditions. The plasma lacks a short-range order by virtue of its ionization composition, and is characterized by Braginsky e-i coupling value (Braginskii *et al.*, 1965); originally derived by Kogan (1959). Plasma e-i coupling value is limited by the maximal possible coupling constraint (Fisher, 2005b) due to a limit on energy transfer in a single e-i collision. (The maximal possible coupling value is evaluated by simply assuming a large-angle elastic scattering of

electrons on ions, with a MFP equal to the interionic distance). As the plasma e-i energy coupling constant is typically an order of magnitude larger than e-i (or, more accurately, e-ph) energy coupling constant of a simple metal, one would expect a notable shortening in ultrafast melting times of a charge-disordered metal in comparison to a model in which the charge disorder is disregarded. A comparison for Cu between melting times with and without an account for the charge disorder is given in Figure 1 of (Fisher, 2005b). Charge disorder in Cu is discussed in the next Section.

8. CHARGE DISORDER IN NOBLE METALS

The occurrence of charge disorder was first predicted by Fisher *et al.* (2004, 2005a, 2005b) for noble metals under ultrashort pulse laser irradiation. In noble metals (Cu, Ag, Au) the charge disorder is brought along by a mechanism that is somewhat different from that in the normal metals described above. In normal metals, charge disorder is brought along by core state vacancies production, the core state being localized throughout the T_e range considered. In noble metals, on the other hand, charge disorder is brought along by d-band state localization which occurs at T_e values of a few electron-volts. At room temperature, d-band hole is mobile, similar to a conductivity-band hole, rather than localized in a single ion potential well. The criterion for mobile *versus* localized holes is according to the relationship between (A) hole tunneling rate out of the resonance and (B) the hole inverse lifetime with respect to inelastic processes. At room temperature, in d-bands of noble metals the typical hole inelastic lifetimes (dominated by three-body recombination) are 5 – 50 fs, see for example, Zhukov *et al.* (2003). We estimate the room-temperature tunneling time to be of order of 1 fs, so the holes are not localized. As T_e increases, binding energy of the d-band increases with it, and the d-hole tunneling rate between individual ion sites drops. This leads to localization of the d-holes at individual lattice sites. In the localization T_e domain, T_e of a few eV, the d-band hole concentration is already large. It exceeds one hole per ion at $T_e \gtrsim 3$ eV, see Table 4. Thus, the charge disorder follows directly from d-band localization. In other words, in noble metals charge disorder is brought along by a collective process (band structure evolution with increasing

Table 4. Equilibrium number of electrons per ion in d-bands of noble metals, as a function of electron temperature at solid density, evaluated using INFERNO model

Element (band)	T_e			
	3 eV	5 eV	7 eV	10 eV
Cu (3d)	9.0	8.7	8.3	7.5
Ag (4d)	9.0	8.5	7.9	7.1
Au (5d)	8.7	8.3	7.8	7.1

T_e) rather than by inelastic pair collisions (EII events) as in normal metals. As the result, in noble metals the parameters governing the eMPT are the energy $E(T_e)$ and the lifetime width of the d-band, while in normal metals the parameter governing eMPT is the core-state vacancy abundance. Moreover, during a femtosecond laser irradiation of normal metals with large E_b , the core state population is not necessarily in thermal equilibrium with the conductivity-band electrons. In that case, the core-state vacancy abundance depends on time explicitly (and not via T_e), and is determined by the ionization rate.

9. INTERMEDIATE CASES

The metals Zn, Cd, Sn, and Pb represent an intermediate case between noble metals on one hand and normal metals on the other. The d-bands of Zn and Cd are located close to the bottom of the conductivity band, and are localized in the above sense even at room temperature. In the case of Zn and Cd Eq. (12) is inapplicable. In Sn (white tin) and in Pb, the fully occupied d-bands are located several electron-volts below the bottom of the conductivity band, $E_b \approx E_F \approx 10$ eV. For Sn and Pb, Eq. (12) can be applied, provided an amenable Y calibration is carried out. Such a procedure is, however, largely unnecessary. Indeed, due to the relative proximity in energy between the d-band and the conductivity band one can assume that, at least on a time scale of 10 fs or longer, the d-band hole population is in thermal equilibrium with the conductivity electrons. INFERNO model calculation results for average fraction of core-ionized lattice ions, $N_{q-1}/N_i = qh$, in 4d band of Sn and in 5d band of Pb are given in Table 5. One can see that the charge disorder onset is expected at $T_e \approx 3$ eV. At $T_e = 5$ eV the loss of short-range order is complete. These temperatures are by a factor of 2 – 3 lower than the Fermi temperatures of Sn and Pb.

INFERNO model calculation results for average equilibrium fraction of core-ionized lattice ions qh in 3d band of Zn and in 4d band of Cd are given in Table 6. The core-ionized ion abundance in metallic Zn and Cd becomes significant at T_e as low as 1 – 2 eV. A complete charge disorder is expected at $T_e \geq 2$ eV. For comparison, Fermi energy of Zn is 9.4 eV. Zn thus seems to be the best candidate for charge disorder effect observation using optical lasers. The Fermi energy of Cd is 7.5 eV, so Cd should also exhibit clearly the optical properties characteristic of charge disorder (resistivity saturation) at $T_e \geq 2$ eV.

Table 5. Equilibrium fraction of core-ionized ions in Sn and Pb at solid densities

	$T_e = 2$ eV	$T_e = 3$ eV	$T_e = 4$ eV	$T_e = 5$ eV
qh of Sn 4d state	3×10^{-4}	0.01	0.06	0.2
qh of Pb 5d state	4×10^{-3}	0.05	0.2	0.4

Table 6. Equilibrium fraction of core-ionized ions in Zn and Cd at solid densities

	$T_e = 1.0$ eV	$T_e = 1.5$ eV	$T_e = 2.0$ eV	$T_e = 2.5$ eV
qh of Zn 3d state	5×10^{-3}	0.06	0.16	0.29
qh of Cd 4d state	2×10^{-3}	0.03	0.12	0.24

10. DISCUSSION AND CONCLUSIONS

Transition from metallic to plasma electron transport properties, eMPT, has been studied in metals undergoing ultrashort pulse electromagnetic energy deposition. The mechanisms contributing to eMPT have been discussed, and the role of charge disorder phenomenon in the eMPT has been determined. Approximate analytic expressions for cross-section, probability, and rate of EII of core states, applicable to both metals and plasmas, have been derived. Probability of three-body recombination was determined through detailed balance. Calculations were carried out for a number of normal metals.

It was shown that the charge disorder occurs at room densities in all metals considered. Under equilibrium conditions for core population, in Li, Be, Na, Mg, Al, K, and Ca the charge disorder occurs at temperatures close to Fermi temperature, when the electron momentum relaxation rate is already close to resistivity saturation limit. The resistivity saturation in those metals is reached, with rising electron temperature, due to an increasing electron elastic collision rate. For Zn, Cd, Sn, and Pb the charge disorder occurs at temperatures a few times lower than the Fermi temperature, with charge disorder leading to resistivity saturation. For noble metals, resistivity saturation is also reached through charge disorder. In the case of noble metals, in contrast to simple metals, charge disorder occurs due to d-band sinking and localization, rather than due to core state ionization. It was concluded that effect of charge disorder on visible or near-infrared femtosecond laser absorption coefficient should be pronounced in Zn, Cd, Sn, Pb, Cu, Ag, Au, and probably can not be detected in Li, Be, Na, Mg, Al, K, and Ca. Charge disorder produced directly by energetic photon ionization of core states was also considered. Core hole lifetimes (with respect to recombination from conductivity band) were found to be 10 – 100 fs for $T_e = 0 - 20$ eV and $E_b = 15 - 100$ eV.

Differences in experimentally determined optical properties of Cu and Al near the resistivity saturation domain were noted by Price *et al.* (1995), and the shift of Cu d-band was proposed as an explanation. Lack of detectable effect of core ionization on optical properties of Al was determined both experimentally and theoretically by Fisher *et al.* (2002). In both works, the absorption of visible or near-infrared femtosecond laser pulses was used both to heat the target and to probe its electron transport properties. Unfortunately, we are not aware of any detailed experiment on the femtosecond laser absorption in Zn, Cd, Sn, or Pb that would allow to test the predictions of the present work.

In noble metals, as we said, the charge disorder is expected to increase the value of electron-ion energy coupling coefficient g and thus to reduce melting time. The charge disorder at sub-Fermi temperatures also affects optical properties of the noble metals, although that effect may be somewhat harder to single out. Pump-probe results for Cu were reported in several works. In the pioneering study of Elsayed-Ali *et al.* (1987) Fermi level smearing effect with increasing T_e was demonstrated, for $T_e \leq 0.2$ eV. In a recent study (Sandhu *et al.*, 2005) detailed pump-probe results for Cu and Al are presented for pump intensity of 3×10^{15} W/cm², showing a transition to plasma regime. This intensity produces peak T_e several times higher than the Fermi temperature. For the present purpose (to study the specifics of the eMPT, that is), this temperature is too high. Experiments at 10–100 times lower intensities are needed. In Wang *et al.* (1994) an increase in g was indeed observed by means of a two-pulse thermionic emission, for Au at modest laser intensities (T_e of about 1 eV or even lower). This result is suggestive of a charge disorder effect, however, the temperature seems too low. Thus, the experimental evidence for charge disorder in the noble metals remains inconclusive so far.

Several experiments can be carried out to test the predictions made in this work. First of all, pump-probe or self-absorption ultrashort laser experiments can be carried out on Zn targets in visible or near infrared range. Excessive electron momentum relaxation rate at $T_e > 1$ eV, and resistivity saturation at $T_e \approx 2$ eV are predicted as a result of charge disorder. Similar experiments on Cd are also possible, as explained in the previous Section. For Sn and Pb, the charge disorder is predicted to cause resistivity saturation at $T_e \approx 3$ eV. Experiments with probe wavelength near parallel-band interband absorption peak (the peak being produced by conductivity band splitting at Brillouin zone boundary (Ashcroft *et al.*, 1971)) should be particularly conclusive, since the peak is destroyed by the loss of short-range order in a charge disordered solid. Note that, by contrast, an interband absorption peak produced by electron excitation from a core state or from a d-band to the Fermi surface is not likely to be destroyed by charge disorder. It is subjected, however, to an increased lifetime broadening as a result of an increased electron collision rate; it is also broadened by Fermi level smearing.

Another possibility is to detect the charge disorder effect in ultrafast melting experiments. The X-ray probe experiments (see Siders *et al.*, 1999; von der Linde *et al.*, 2001; Lindenberg *et al.*, 2005) or electron-beam probe experiments (Siwick *et al.*, 2003) allow to directly probe the ion spatial arrangement and to resolve the ultrafast homogeneous or heterogeneous melting dynamics. Those are especially relevant for noble metals where a significant difference in melting times with and without charge disorder is predicted; and for normal metals where, at T_e close to Fermi temperature, various theoretical predictions for electron-ion coupling coefficient value differ substantially.

ACKNOWLEDGMENTS

The authors thankfully acknowledge discussions with Z. Zinamon, S. I. Anisimov, N. A. Inogamov, and S. N. Gordienko.

REFERENCES

- ABRIKOSOV, A.A. (1972). *Introduction to the Theory of Normal Metals*. New York: Academic Press.
- ALESINI, D., BERTOLUCCI, S., BIAGINI, BONI, R., BOSCOLO, M., *et al.* (2004). The SPARC/X SASE-FEL projects. *Laser Part. Beams* **22**, 341–350.
- ALMBLADH, C.-O., MORALES, A.L. & GROSSMANN, G. (1989). Theory of Auger core-valence-valence processes in simple metals. I. Total yields and core-level lifetime widths. *Phys. Rev. B* **39**, 3489–3502.
- ANISIMOV, S.I., BONCH-BRUEVICH, A.M., EL-YASHEVICH, M.A., IMAS, YA.A., PAVLENKO, N.A. & ROMANOV, G.S. (1967). The action of powerful light on metals. *Sov. Phys. Tech. Phys.* **11**, 945–952.
- ANISIMOV, S.I., KAPELIOVICH, B.L. & PERELMAN, T.L. (1974). Electron emission from the surface of metals under the action of ultrashort laser pulses. *Sov. Phys. JETP* **39**, 375–377.
- ASHCROFT, N.W. & STURM, K. (1971). Interband absorption and the optical properties of polyvalent metals. *Phys. Rev. B* **3**, 1898–1910.
- ASHITKOV, S.I., AGRANAT, M.B., KONDRATENKO, P.S., ANISIMOV, S.I., FORTOV, V.E., TEMNOV, V.V., SOKOLOWSKI-TINTEN, K., RETHFELD, B., ZHOU, P. & VON DER LINDE, D. (2002). Ultra-fast laser-induced phase transitions in tellurium. *JETP Lett.* **76**, 461–464.
- BENNEMANN, K.H. (2004). Ultrafast dynamics in solids. *J. Phys. Cond. Matt.* **16**, R995–R1056.
- BRAGINSKII, S.I. (1965). Transport processes in a plasma. In *Reviews of Plasma Physics*, vol. 1. New York: Consultants Bureau.
- CAMPILLO, I., SILKIN, V.M., PITARKE, J.M., CHULKOV, E.V., RUBIO, A. & ECHENIQUE, P.M. (2000). First-principles calculations of hot-electron lifetimes in metals. *Phys. Rev. B* **61**, 13484–13492.
- CAVALLERI, A., SIDERS, C.W., ROSE-PETRUCK, C., JIMENEZ, R., TOTH, Cs., SQUIER, J.A., BARTY, C.P.J., WILSON, K.R., SOKOLOWSKI-TINTEN, K., HORN VON HOEGEN, M., VON DER LINDE, D. (2001). Ultrafast x-ray measurement of laser heating in semiconductors: Parameters determining the melting threshold. *Phys. Rev. B* **63**, 193306.
- CITRIN, P.H., WERTHEIM, G.K. & SCHLUETER, M. (1979). One-electron and many-body effects in X-ray absorption and emission edges of Li, Na, Mg, and Al metals. *Phys. Rev. B* **20**, 3067–3114.
- DUMITRICA, T. & ALLEN, R.E. (2002). Nonthermal transition of GaAs in ultra-intense laser radiation field. *Laser Part. Beams* **20**, 237–242.
- DECAMP, M.F., REIS, D.A., BUCKSBAUM, P.H. & MERLIN, R. (2001). Dynamics and coherent control of high-amplitude optical phonons in bismuth. *Phys. Rev. B* **64**, 092301.
- DHARMA-WARDANA, M.W.C. & PERROT, F. (1998). Energy relaxation and the quasiequation of state of a dense two-temperature nonequilibrium plasma. *Phys. Rev. E* **58**, 3705–3718.
- DHARMA-WARDANA, M.W.C. & PERROT, F. (2001). Erratum. *Phys. Rev. E* **63**, 069901.

- EIDMANN, K., MEYER-TER-VEHN, J., SCHLEGEL, T. & HUELLER, S. (2000). Hydrodynamic simulation of subpicosecond laser interaction with solid-density matter. *Phys. Rev. E* **62**, 1202–1214.
- ELIEZER, S. (2002). *The Interaction of High-Power Lasers with Plasmas*. Bristol: IoP Publications.
- ELIEZER, S., ELIAZ, N., GROSSMAN, E., FISHER, D., GOUZMAN, I., PECKER, S., HOROVITZ, Y., FRAENKEL, M., MAMAN, S., EZERSKY, V. & ELIEZER, D. (2005). Nanoparticles and nanotubes induced by femtosecond lasers. *Laser Part. Beams* **23**, 15–19.
- ELSAIED-ALI, H.E., NORRIS, T.B., PESSOT, M.A. & MOUROU, G.A. (1987). Time-resolved observation of electron-phonon relaxation in copper. *Phys. Rev. Lett.* **58**, 1212–1215.
- FERMI, E. (1940). The ionization loss of energy in gases and in condensed materials. *Phys. Rev.* **57**, 485–493.
- FIRST, P.N., FINK, R.L. & FLYNN, C.P. (1988). Emission spectra and core-hole lifetimes from anomalous X-ray edges in alloys. *Phys. Rev. Lett.* **60**, 952–955.
- FISHER, D., FRAENKEL, M., HENIS, Z., MOSHE, E. & ELIEZER, S. (2002). Interband and intraband (Drude) contributions to femtosecond laser absorption in aluminum. *Phys. Rev. E* **65**, 016409.
- FISHER, D., FRAENKEL, M., ZINAMON, Z., HENIS, Z., MOSHE, E., HOROVITZ, Y., LUZON, E., MAMAN, S. & ELIEZER, S. (2004) in ECLIM-XXVIII proceedings, Rome, 2004.
- FISHER, D., FRAENKEL, M., ZINAMON, Z., HENIS, Z., MOSHE, E., HOROVITZ, Y., LUZON, E., MAMAN, M. & ELIEZER, S. (2005). Intraband and interband absorption of femtosecond laser pulses in copper. *Laser Part. Beams* **23**, 391–393.
- FISHER, D., HENIS, Z. & ZINAMON, Z. (2005). *GSI Annual Report 2004 on High Energy Density Physics with Intense Laser and Ion Beams* (Weyrich, K. & Hoffmann, D.H.H., eds.). Darmstadt, Germany: GSI.
- GAMALY, E.G., RODE, A. V., LUTHER-DAVIES, B. & TIKHONCHUK, V. T. (2002). Ablation of solids by femtosecond lasers: Ablation mechanism and ablation thresholds for metals and dielectrics. *Phys. Plasmas* **9**, 949–957.
- GAMBIRASIO, A., BERNASCONI, M. & COLOMBO, L. (2000). Laser-induced melting of silicon: A tight-binding molecular dynamics simulation. *Phys. Rev. B* **61**, 8233–8237.
- GERICKE, D.O., MURILLO, M.S. & SCHLANGES, M. (2002). Dense plasma temperature equilibration in the binary collision approximation. *Phys. Rev. E* **65**, 036418.
- GRIEM, H.R. (1997). *Principles of Plasma Spectroscopy*. Cambridge, UK: Cambridge University Press.
- GUO, C., RODRIGUEZ, G., LOBAD, A. & TAYLOR, A.J. (2000). Structural phase transition of aluminum induced by electronic excitation. *Phys. Rev. Lett.* **84**, 4493–4496.
- HAZAK, G., ZINAMON, Z., ROSENFELD, Y. & DHARMA-WARDANA, M.W.C. (2001). Temperature relaxation in two-temperature states of dense electron-ion systems. *Phys. Rev. E* **64**, 066411.
- HOFFMANN, D.H.H., BLAZEVIC, A., NI, P., ROSMEJ, O., ROTH, M., TAHIR, N.A., TAUSCHWITZ, A., UDREA, S., VARENTSOV, D., WEYRICH, K. & MARON, Y. (2005). Present and future perspectives for high energy density physics with intense heavy ion and laser beams. *Laser Part. Beams* **23**, 47–53.
- HUNSCHKE, S., WIENECKE, K., DEKORSY, T. & KURZ, H. (1995). Impulsive Softening of Coherent Phonons in Tellurium. *Phys. Rev. Lett.* **75**, 1815–1818.
- INOKUTI M. & SMITH, D.Y. (1982). Fermi density effect on the stopping power of metallic aluminum. *Phys. Rev. B* **25**, 61–66.
- JESCHKE, H.O., GARCIA, M.E. & BENNEMANN, K.H. (2001). Theory for the ultrafast ablation of graphite films. *Phys. Rev. Lett.* **87**, 015003.
- JOHANSSON, B. & MARTENSSON, N. (1980). Core-level binding-energy shifts for the metallic elements. *Phys. Rev. B* **21**, 4427–4457.
- KE LAN, F. E. & MEYER-TER-VEHN, J. (2004). Photopumping of XUV lasers by XFEL radiation. *Laser Part. Beams* **22**, 261–266.
- KEMP, A., PFUND, R.E.W. & MEYER-TER-VEHN, J. (2004). Modeling ultrafast laser-driven ionization dynamics with Monte Carlo collisional particle-in-cell simulations. *Phys. Plasmas* **11**, 5648–5657.
- KNORREN, R., BOUZERAR, G. & BENNEMANN, K.H. (2001). Dynamics of excited electrons in copper: The role of Auger electrons. *Phys. Rev. B* **63**, 094306.
- KOGAN, V.I. (1959). *Plasma Physics and the Problem of Controlled Thermonuclear Reactions*, vol. 1. New York: Pergamon Press.
- LEE, Y.T. & MORE, R.M. (1984). An electron conductivity model for dense plasmas. *Phys. Fluids* **27**, 1273–1286.
- LEE, R.W., BALDIS, H.A., CAUBLE, R.C., LANDEN, O.L., WARK, J.S., NG, A., ROSE, S.J., LEWIS, C., RILEY, D., GAUTHIER, J.-C. & AUDEBERT, P. (2002). Plasma-based studies with intense X-ray and particle beam sources. *Laser Part. Beams* **20**, 527–536.
- LIBERMAN, D.A. (1979). Self-consistent field model for condensed matter. *Phys. Rev. B* **20**, 4981–4989.
- LIBERMAN, D.A. (1982). INFERNO: A better model of atoms in dense plasmas. *J. Quant. Spectrosc. Radiat. Transfer* **27**, 335–339.
- LINDENBERG, A.M., et al. (2005). Atomic-scale visualization of inertial dynamics. *Science* **308**, 392–395.
- MALKA, V. & FRITZLER, S. (2004). Electron and proton beams produced by ultra short laser pulses in the relativistic regime. *Laser Part. Beams* **22**, 399–405.
- MILCHBERG, H.M., FREEMAN, R.R., DAVEY, S.C. & MORE, R.M. (1988). Resistivity of a simple metal from room temperature to 10^6 K. *Phys. Rev. Lett.* **61**, 2364–2367.
- MOTT, N.F. (1990). *Metal-Insulator Transitions*, 2nd ed. London: Taylor-Francis Ltd.
- MURILLO, M.S. & WEISHEIT, J.C. (1998). Dense plasmas, screened interactions, and atomic ionization. *Phys. Rep.* **302**, 1–65.
- NEDDERMEYER, H. (1976). X-ray emission and absorption edges of magnesium and aluminum. *Phys. Rev. B* **13**, 2411–2417.
- NG, A., CELLIERS, P., FORSMAN, A., MORE, R.M., LEE, Y.T., PERROT, F., DHARMA-WARDANA, M.W.C. & RINKER, G.A. (1994). Reflectivity of intense femtosecond laser pulses from a simple metal. *Phys. Rev. Lett.* **72**, 3351–3354.
- NOZIERES P. & PINES D. (1959). Electron interaction in solids. Characteristic energy loss spectrum. *Phys. Rev.* **113**, 1254–1267.
- PAL'CHIKOV, V.G. & SHEVELKO, V.P. (1995). *Reference Data on Multicharged Ions*. Berlin: Springer Verlag.
- PRICE, D.F., MORE, R.M., WALLING, R.S., GUETHLEIN, G., SHEPHERD, R.L., STEWART, R.E. & WHITE, W.E. (1995). Absorption of ultrashort laser pulses by solid targets heated rapidly to temperatures 1–1000 eV. *Phys. Rev. Lett.* **75**, 252–255.
- REITZE, D.H., AHN, H. & DOWNER, M.C. (1992). Optical properties of liquid carbon measured by femtosecond spectroscopy. *Phys. Rev. B* **45**, 2677–2693.
- RETHFELD, B., SOKOLOWSKI-TINTEN, K., VON DER LINDE, D. & ANISIMOV, S.I. (2002). Ultrafast thermal melting of laser-excited solids by homogeneous nucleation. *Phys. Rev. B* **65**, 092103.

- RETHFELD, B., TEMNOV, V.V., SOKOLOWSKI-TINTEN, K., TSU, P., VON DER LINDE, D., ANISIMOV, S. I., ASHITKOV, S.I. & AGRANAT, M.B. (2004). Superfast thermal melting of solids under the action of femtosecond laser pulses. *J. Opt. Techn.* **71**, 348–352.
- SAETA, P., WANG, J.-K., SIEGAL, Y., BLOEMBERGEN, N. & MAZUR, E. (1991). Ultrafast electronic disordering during femtosecond laser melting of GaAs. *Phys. Rev. Lett.* **67**, 1023–1026.
- SALZMANN, D. (1998). *Atomic Physics in Hot Plasmas*. New York: Oxford University Press.
- SANDHU, A.S., DHARMADHIKARI, A.K. & KUMAR, G.R. (2005). Time resolved evolution of structural, electrical, and thermal properties of copper irradiated by an intense ultrashort laser pulse. *J Appl. Phys.* **97**, 023526.
- SCHOENE, W.-D., KEYLING, R., BANDIC, M. & EKARDT, W. (1999). Calculated lifetimes of hot electrons in aluminum and copper using a plane-wave basis set. *Phys. Rev. B* **60**, 8616–8623.
- SHANK, C.V., YEN, R. & HIRLIMANN, C. (1983). Femtosecond-time-resolved surface structural dynamics of optically excited silicon. *Phys. Rev. Lett.* **51**, 900–902.
- SIDERS, C.W., CAVALLERI, A., SOKOLOWSKI-TINTEN, K., TOTH, Cs., GUO, T., KAMMLER, M., HORN VON HOEGEN, M., WILSON, K.R., VON DER LINDE, D. & BARTY, C.P.J. (1999). Detection of non-thermal melting by ultrafast X-ray diffraction. *Science* **286**, 1340–1342.
- SILVESTRELLI, P.L., ALAVI, A., PARRINELLO, M. & FRENKEL, D. (1996). Ab initio molecular dynamics simulation of laser melting of silicon. *Phys. Rev. Lett.* **77**, 3149–3152.
- SIWICK, B.J., DWYER, J.R., JORDAN, R.E. & MILLER, R.J.D. (2003). An atomic-level view of melting using femtosecond electron diffraction. *Science* **302**, 1382–1385.
- SOKOLOWSKI-TINTEN, K., BIALKOWSKI, J. & VON DER LINDE, D. (1995). Ultrafast laser-induced order-disorder transitions in semiconductors. *Phys. Rev. B* **51**, 14186–14198.
- SOKOLOWSKI-TINTEN, K., BIALKOWSKI, J., BOING, M., CAVALLERI, A. & VON DER LINDE, D. (1998). Thermal and non-thermal melting of gallium arsenide after femtosecond laser excitation. *Phys. Rev. B* **58**, R11805–R11808.
- STAMPFLI, P. & BENNEMANN, K.H. (1992). Dynamical theory of the laser-induced lattice instability of silicon. *Phys. Rev. B* **46**, 10686–10692.
- STERNHEIMER, R.M. & PEIERLS, R.F. (1971). General expression for the density effect for the ionization loss of charged particles. *Phys. Rev. B* **3**, 3681–3692.
- THEIS, W. & HORN, K. (1993). Temperature-dependent line broadening in core-level photoemission spectra from aluminum. *Phys. Rev. B* **47**, 16060–16063.
- TOM, H.W.K., AUMILLER, G.D. & BRITO-CRUZ, C.H. (1988). Time-resolved study of laser-induced disorder of Si surfaces. *Phys. Rev. Lett.* **60**, 1438–1441.
- UTEZA, O.P., GAMALY, E.G., RODE, A.V., SAMOC, M. & LUTHER-DAVIES, B. (2004). Gallium transformation under femtosecond laser excitation: Phase coexistence and incomplete melting. *Phys. Rev. B* **70**, 054108.
- VON DER LINDE, D., SOKOLOWSKI-TINTEN, K., BLOME, CH., DIETRICH, C., ZHOU, P., TARASEVITCH, A., CAVALLERI, A., SIDERS, C.W., BARTY, C.P.J., SQUIER, J., WILSON, K.R., USCHMANN, I., FOERSTER, E. (2001). Generation and application of ultrashort X-ray pulses. *Laser Part. Beams* **19**, 15–22.
- WANG, X.Y. & DOWNER, M.C. (1992). Femtosecond time-resolved reflectivity of hydrodynamically expanding metal surfaces. *Opt. Lett.* **17**, 1450–1452.
- WANG, X.Y., RIFFE, D.M., LEE, Y.-S., DOWNER, M.C. (1994). Time-resolved electron-temperature measurement in a highly excited gold target using femtosecond thermionic emission. *Phys. Rev. B* **50**, 8016–8019.
- YOUN, S.J., MIN, B.I., RHO, T.H. & KIM, K.S. (2004). Nested Fermi surfaces, optical peaks, and laser-induced structural transition in Al. *Phys. Rev. B* **69**, 033101.
- ZHUKOV, V.P., CHULKOV, E.V. & ECHENIQUE, P.M. (2003). Lifetimes of d holes in Cu and Au: Full-potential LMTO approach. *Phys. Rev. B* **68**, 045102.